

# Multi-Modal Representation Learning via Semi-Supervised Rate Reduction for Generalized Category Discovery

Wei He<sup>†</sup>, Xianghan Meng<sup>†</sup>, Zhiyuan Huang<sup>†</sup>, Xianbiao Qi<sup>‡</sup>, Rong Xiao<sup>‡</sup>, Chun-Guang Li<sup>\*,†</sup>

<sup>†</sup> School of Artificial Intelligence, Beijing University of Posts and Telecommunications

{wei.he, huangzhiyuan, mengxianghan, lichunguang}@bupt.edu.cn

<sup>‡</sup> Intellifusion Inc., Shenzhen, P.R. China

## Abstract

*Generalized Category Discovery (GCD) aims to identify both known and unknown categories, with only partial labels given for the known categories, posing a challenging open-set recognition problem. State-of-the-art approaches for GCD task are usually built on multi-modality representation learning, which is heavily dependent upon inter-modality alignment. However, few of them cast a proper intra-modality alignment to generate a desired underlying structure of representation distributions. In this paper, we propose a novel and effective multi-modal representation learning framework for GCD via Semi-Supervised Rate Reduction, called SSR<sup>2</sup>-GCD, to learn cross-modality representations with desired structural properties based on emphasizing to properly align intra-modality relationships. Moreover, to boost knowledge transfer, we integrate prompt candidates by leveraging the inter-modal alignment offered by Vision Language Models. We conduct extensive experiments on generic and fine-grained benchmark datasets demonstrating superior performance of our approach.*

## 1. Introduction

Generalized Category Discovery (GCD) has emerged as a natural and challenging extension of open-set recognition with the aim of discovering categories (i.e., patterns) in the open world [17, 20]. The goal of GCD is to recognize both known and unknown categories, going beyond the standard open-set recognition problem by leveraging knowledge learned from known categories to discover unknown categories. For example, in the typical setting of GCD task, half of categories are partially labeled (known) and the rest of categories remain unlabeled (unknown). Such a setting is relevant to real-world exploration scenarios in which data exhibit a mixture of known and unknown class structures.

Roughly speaking, the existing state-of-art approaches to address the GCD problem usually follow a two-phases

framework: a) generating representations for images by fine-tuning the pre-trained models, and b) applying clustering algorithms on the learned representations of all unlabeled data. However, these approaches lack of effective signals to transfer knowledge from known categories to discovering unknown categories, that is, almost all of them are using the given partial labels to recognize the known categories but recover the unknown categories in unsupervised or self-supervised manner.

For our human being, it is consciously or unconsciously leveraging information or cues of multiple sources from known categories to recognize unknown categories. Recently, there are a few attempts to explore multi-modal frameworks for GCD in image modality by integrating information from textual modality. For example, CLIP-GCD [13] leverages a knowledge database to search for similar texts of query images, TextGCD [30] constructs prompts from tag and attribute lexicons, and GET [22] learns a textual inversion network to generate prompts. These frameworks for multi-modal GCD have exploited textual cues into visual datasets to perform inter-modality alignment for cross-modality representation learning, but lack sufficient consideration on the underlying structure of the distribution in the learned representation. For example, an existing CLIP-style inter-modality loss [15] or a GCD-style intra-modality loss [20] is incorporated to conduct inter-modality alignment for representation learning, lacking of a proper loss for intra-modality alignment. Thus clear insights into the role of inter-modality and intra-modality interactions are still vague.

In this paper, we attempt to incorporate the maximal coding rate reduction principle [26] for multi-modality representation learning, and present a novel and efficient framework, called Semi-Supervised Rate Reduction (SSR<sup>2</sup>) for GCD (SSR<sup>2</sup>-GCD for short). To be specific, in SSR<sup>2</sup>-GCD, a so-called Semi-Supervised Rate Reduction (SSR<sup>2</sup>) loss is used to learn structured representations, in which the consistency of intra-modal representations is encouraged. Unlike the existing multi-modal GCD approaches, in our

SSR<sup>2</sup>-GCD, the learned cross-modality representations for both known and unknown categories are compressed into evenly distributed structure. This finding is thoroughly discussed and validated through extensive experiments. Moreover, we also present a Retrieval-based Text Aggregation (RTA) strategy to enhance the text generation, in which the information from a larger amount of prompt candidates is integrated to generate semantic-rich textual representations. **Paper Contributions.** The main contributions of the paper are highlighted as follows.

1. We propose a Semi-Supervised Rate Reduction framework for Generalized Category Discovery (SSR<sup>2</sup>-GCD) to learn structured representations with desired distribution structures.
2. We present an effective Retrieval-based Text Aggregation (RTA) strategy for generating semantic-rich representations to boost knowledge transfer.
3. We conduct extensive experiments on eight datasets, showing superior performance of the proposed approach.

## 2. Preliminaries

### 2.1. Problem Notation

Denote the data set as  $\mathcal{D}_L \cup \mathcal{D}_U$ , which consists of labeled data  $\mathcal{D}_L = (\mathbf{x}_i, \mathbf{y}_i^l)_{i=1}^M \subseteq \mathcal{X} \times \mathcal{Y}_L$  and unlabeled data  $\mathcal{D}_U = (\mathbf{x}_i, \mathbf{y}_i^u)_{i=1}^N \subseteq \mathcal{X} \times \mathcal{Y}_U$ , where  $\mathcal{Y}_L$  and  $\mathcal{Y}_U$  denote the label spaces, and  $\mathcal{Y}_L \subset \mathcal{Y}_U$ . In the GCD setting, the labeled samples in  $\mathcal{D}_L$  are from the known categories; whereas unlabeled samples in  $\mathcal{D}_U$  are either from the known categories nor from some unknown categories. As usual, the total number of categories  $K = |\mathcal{Y}_U|$  is given or can be estimated. The goal of GCD is to estimate the labels of samples in  $\mathcal{D}_U$ .

### 2.2. Multi-modal GCD Pipelines

In this section, we review the pipeline for multi-modal GCD closely relevant to our approach. The common practice of multi-modal GCD frameworks consist of three components: text generation, representation learning, and clustering.

**Text Generation.** To introduce textual cues to visual datasets, inherent inter-modal alignment capability of pre-trained VLMs is leveraged to generate pseudo-texts for query images. Among these approaches, retrieval-based methods [9, 30] construct a prompt database  $\mathcal{P}$  and search for the optimal prompt  $p \in \mathcal{P}$  that maximizes the cosine similarity between the embeddings of query image and prompt candidates. For instance, TextGCD [30] uses the class names in ImageNet [4] to construct the tag lexicon and leverages GPT3 [2] to generate distinguishing attributes for these tags. For each query image, the top-3 similar tags and top-2 similar attributes are used to construct the prompt: “most likely {tag<sub>1</sub>}, perhaps {tag<sub>2</sub>}, likely {tag<sub>3</sub>}, most

likely {attr<sub>1</sub>}, perhaps {attr<sub>2</sub>}”.

**Representation Learning.** Given query images and their corresponding pseudo-texts, multi-modal GCD frameworks usually refine their representations simultaneously. For instance, TextGCD [30] learns the representations by simply following the CLIP-style inter-modal contrastive loss, i.e.,

$$\mathcal{L}_{\text{CLIP}} = -\frac{1}{|B|} \sum_{i \in B} \log \frac{\exp(\mathbf{z}_i^{\text{I}\top} \mathbf{z}_i^{\text{T}} / \tau_c)}{\sum_{j \neq i} \exp(\mathbf{z}_i^{\text{I}\top} \mathbf{z}_j^{\text{T}} / \tau_c)}, \quad (1)$$

where  $B$  denotes the mini-batch of data,  $\mathbf{z}_i^{\text{I}}, \mathbf{z}_i^{\text{T}} \in \mathbb{R}^d$  denote the embeddings of  $i$ -th image and pseudo-text, and  $\tau_c$  is the temperature factor. Optimizing both  $\mathcal{L}_{\text{CLIP}}$  and objectives encourages the inter-modal alignment between image and text manifolds, but does not account for intra-modal alignment within each modality. GET [22] also encourages the inter-modal alignment in representation learning, while incorporating the widely-used supervised and unsupervised contrastive losses to align intra-modal relationships within each modality, i.e.,

$$\begin{aligned} \mathcal{L}_{\text{con}} &= \lambda \mathcal{L}_{\text{con}}^{\text{s}} + (1 - \lambda) \mathcal{L}_{\text{con}}^{\text{u}}, \\ \mathcal{L}_{\text{con}}^{\text{s}} &= -\sum_{i \in B_i} \frac{1}{|\mathcal{N}_i|} \sum_{j \in \mathcal{N}_i} \log \frac{\exp(\mathbf{z}_i^{\text{T}\top} \mathbf{z}'_j / \tau_a)}{\sum_{m \neq i} \exp(\mathbf{z}_i^{\text{T}\top} \mathbf{z}'_m / \tau_a)}, \\ \mathcal{L}_{\text{con}}^{\text{u}} &= -\sum_{i \in B} \log \frac{\exp(\mathbf{z}_i^{\text{T}\top} \mathbf{z}'_i / \tau_b)}{\sum_{m \neq i} \exp(\mathbf{z}_i^{\text{T}\top} \mathbf{z}'_m / \tau_b)}, \end{aligned} \quad (2)$$

where  $\lambda$  is the balancing parameter,  $B_\ell$  denotes the labeled subset of  $B$ ,  $\mathbf{z}_i$  and  $\mathbf{z}'_i$  are embeddings of augmented data pairs,  $\mathcal{N}_i$  is data indices with the same label as  $i$ -th data, and  $\tau_a$  and  $\tau_b$  are the temperature parameters. Still, the intra-modal representation learning in multi-modal GCD frameworks adheres to the paradigm of uni-modal counterparts, and fails to resolve the inherent problems of this paradigm. That is, optimizing  $\mathcal{L}_{\text{con}}$  results in the *imbalanced compression* of embeddings, since  $\mathcal{L}_{\text{con}}^{\text{u}}$  pulls positive augmented data pairs across all categories, whereas  $\mathcal{L}_{\text{con}}^{\text{s}}$  further pulls labeled data together only for known categories. As illustrated in Figure 1, such an imbalanced compression issue prevents clustering algorithms from accurately identifying cluster boundaries.

**Clustering.** Existing multi-modal GCD frameworks usually follow SimGCD [25] for clustering unlabeled data, which consists of a supervised cross-entropy loss [7] and an unsupervised self-distillation loss [1], i.e.,

$$\mathcal{L}_{\text{cls}} = \sum_{i \in B_i} \ell_{\text{CE}}(\mathbf{y}_i^*, \mathbf{y}_i) + \gamma \sum_{i \in B} \ell_{\text{CE}}(\mathbf{y}'_i, \mathbf{y}_i) - \mu H(\bar{\mathbf{y}}), \quad (3)$$

where  $\gamma$  and  $\mu$  are the balancing parameters,  $\ell_{\text{CE}}$  denotes the cross-entropy loss,  $\mathbf{y}_i^*$  is the ground-truth label of the

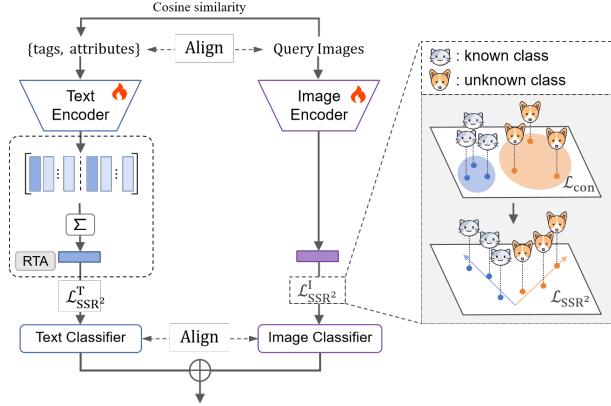


Figure 1. Illustration of Our Proposed Framework: SSR<sup>2</sup>-GCD.

$i$ -th image,  $\mathbf{y}_i$  is the prediction of the  $i$ -th embedding  $\mathbf{z}_i$ ,  $\mathbf{y}'_i$  is the prediction of the augmented counterpart  $\mathbf{z}'_i$  with a sharper temperature in  $\text{SOFTMAX}$ . The mean entropy regularizer [19]  $H(\bar{\mathbf{y}}) = -\sum_k \bar{\mathbf{y}}^{(k)} \log \bar{\mathbf{y}}^{(k)}$  is introduced to prevent degenerated predictions in new categories, where  $\bar{\mathbf{y}} = \frac{1}{2|B|} \sum_{i \in B} (\mathbf{y}_i + \mathbf{y}'_i)$  denotes the mean prediction of  $\mathbf{y}_i + \mathbf{y}'_i$  in a mini-batch using the same temperature, and  $\bar{\mathbf{y}}^{(k)}$  is the value of  $\bar{\mathbf{y}}$  in the  $k$ -th class. For example, GET trains a single MLP by optimizing the loss in Eq.(3) to produce predictions for both image and text embeddings, whereas TextGCD implements dual-branch classifiers to handle image and text embeddings, respectively. Additionally, TextGCD uses the co-teaching strategy, in which high-confidence samples are used to supervise the learning of classifiers, i.e.,

$$\mathcal{L}_{\text{co-teach}} = \sum_{i \in \mathcal{S}^I} \ell_{\text{CE}}(\mathbf{y}_i^I, \mathbf{y}_i^T) + \sum_{j \in \mathcal{S}^T} \ell_{\text{CE}}(\mathbf{y}_j^T, \mathbf{y}_j^I), \quad (4)$$

where  $\mathcal{S}^I, \mathcal{S}^T$  are the sample sets selected based on the confidence score of  $\mathbf{y}^I$  and  $\mathbf{y}^T$ , respectively.

### 3. Our Proposed Approach: SSR<sup>2</sup>-GCD

our proposed framework consists of three modules: a) a Retrieval-based Text Aggregation (RTA) strategy for text generation; b) a set of Semi-Supervised Rate Reduction (SSR<sup>2</sup>) modules for representation learning; and c) a dual-branch classifier to learn pseudo-labels from each modality. Specifically, at first we use RTA to aggregate embeddings of prompts to incorporate textual information that is helpful in discovering unknown categories; then, we use Semi-Supervised Rate Reduction (SSR<sup>2</sup>) modules to learn structured representations with desired properties. The dual-branch classifier is deployed to learn pseudo-labels from each modality. For clarity, we illustrate our proposed framework in Figure 1.

### 3.1. Retrieval-based Text Aggregation

For text generation, we adopt TextGCD [30] to construct tag and attribute lexicons, and then search for similar tags and attributes, since we find that incorporating more information from multiple tag and attribute candidates is helpful in discovering patterns of unknown categories. Still, due to CLIP’s limitation in handling long textual prompts, the way of constructing prompts in TextGCD is sub-optimal, because that CLIP fails to generate satisfactory embeddings for prompts exceeding 20 tokens [27]. Given CLIP’s text encoder  $\mathcal{F}^T$  and tokenizer  $\mathcal{T}$ , instead, in this paper, we use the text encoder to embed tag and attribute prompts, and then compute the textual embedding by:

$$\mathbf{z}^T = \sum_{i=1}^c \sigma_i \mathcal{F}^T(\mathcal{T}(a_i)) + \sum_{i=1}^c \sigma_i \mathcal{F}^T(\mathcal{T}(b_i)), \quad (5)$$

where  $a_i$  and  $b_i$  are the  $i$ -th similar tags and attributes, respectively, as ranked by the cosine similarity between their embeddings and the embedding of query image  $\mathbf{z}^I$ ,  $c$  means that only the top- $c$  most similar tags and attributes are considered, and the variable  $\sigma_i$  assigns higher weights to the most-similar tag and attribute and aggregates information from other candidates, i.e.,

$$\sigma_i = \begin{cases} 1 - \alpha & \text{if } i = 1 \\ \frac{\alpha}{c-1} & \text{otherwise,} \end{cases} \quad (6)$$

where  $\alpha > 0$  is hyper-parameter (e.g.,  $\alpha = 0.5$ ). Such a method allows us to aggregate richer information from a larger set of candidates (e.g.,  $c = 4$ ).

### 3.2. Semi-supervised Rate Reduction Modules for Representation Learning

In this section, we tackle the imbalanced compression issue in existing representation learning methods. Specifically, we propose a Semi-supervised Rate Reduction (SSR<sup>2</sup>) approach to learn structured representations from intra-modal relationships while achieving even compression across known and unknown categories. Inspired by the principle of Maximal Coding Rate Reduction [26], a structured representation learning technique originally developed for supervised settings, we formulate SSR<sup>2</sup> objective as follows:

$$\mathcal{L}_{\text{SSR}^2} = -R(\mathbf{Z}) + R_c^s(\mathbf{Z}, \mathbf{Y}^*) + R_c^u(\mathbf{Z}, \mathbf{Y}), \quad (7)$$

where

$$R(\mathbf{Z}) = \log \det \left( \mathbf{I} + \frac{d}{N\epsilon^2} \mathbf{Z}\mathbf{Z}^\top \right),$$

$$R_c^s(\mathbf{Z}_s, \mathbf{Y}^*) = \frac{1}{N} \sum_{j=1}^k N_j^s \log \det \left( \mathbf{I} + \frac{d}{N_j^s \epsilon^2} \mathbf{Z}_s \text{Diag}(\mathbf{Y}_j^*) \mathbf{Z}_s^\top \right), \quad \mathcal{L}_{\text{warm}} = \mathcal{L}_{\text{SSR}^2}^I + \mathcal{L}_{\text{SSR}^2}^T + \mathcal{L}_{\text{cls}}^I + \mathcal{L}_{\text{cls}}^T. \quad (9)$$

$$R_c^u(\mathbf{Z}_u, \mathbf{Y}) = \frac{1}{N} \sum_{j=1}^k N_j^u \log \det \left( \mathbf{I} + \frac{d}{N_j^u \epsilon^2} \mathbf{Z}_u \text{Diag}(\mathbf{Y}_j) \mathbf{Z}_u^\top \right),$$

where  $\mathbf{Z}$  denotes the embeddings of a mini-batch,  $\mathbf{Z}_s, \mathbf{Z}_u$  are the embeddings of labeled and unlabeled data,  $\mathbf{Y}^*$  denotes ground-truth labels,  $\mathbf{Y}$  denotes the pseudo-labels predicted by classifiers,  $\mathbf{I}$  is the identity matrix,  $k$  is the number of categories,  $\epsilon > 0$  is the hyper-parameter ( $\epsilon = 0.5$  in experiments),  $N_j^s$  is the number of labeled data points assigned by  $\mathbf{Y}^*$  that belong to the  $j$ -th class, and  $N_j^u$  is the number of unlabeled data points assigned by  $\mathbf{Y}$  that belong to the  $j$ -th class.

During training, we fine-tune the image and text encoders of CLIP [15], and the loss for each encoder is analogous to  $\mathcal{L}_{\text{SSR}^2}$ , with the replacement of embedding  $\mathbf{Z}$  and pseudo-labels  $\mathbf{Y}$  by image and text embeddings  $\mathbf{Z}^I, \mathbf{Z}^T$  and pseudo-labels of dual-branch classifiers  $\mathbf{Y}^I, \mathbf{Y}^T$ , i.e.,

$$\begin{aligned} \mathcal{L}_{\text{SSR}^2}^I &= -R(\mathbf{Z}^I) + R_c^s(\mathbf{Z}^I, \mathbf{Y}^*) + R_c^u(\mathbf{Z}^I, \mathbf{Y}^I), \\ \mathcal{L}_{\text{SSR}^2}^T &= -R(\mathbf{Z}^T) + R_c^s(\mathbf{Z}^T, \mathbf{Y}^*) + R_c^u(\mathbf{Z}^T, \mathbf{Y}^T). \end{aligned} \quad (8)$$

The effects of introducing  $\text{SSR}^2$  are twofold. On the one hand, maximizing the term  $R(\cdot)$  in Eq. 7 expands the whole embeddings globally while minimizing the terms  $R_c^s(\cdot)$  and  $R_c^u(\cdot)$  encourages the embeddings of each category to span low-dimensional subspaces with even matrix ranks, as proved in [24, 26]. Owing to such a desired property, the representations in each category are **evenly compressed**. Additionally, the introduced  $\text{SSR}^2$  focuses on aligning intra-modal relationships and accommodate the discrepancies between modalities. We find that the inter-modal alignment leads to **intra-modal misalignment** and can be unnecessary in multi-modal GCD frameworks, as discussed and validated in our experiments. To our knowledge, this is the first work to address the imbalanced compression issue in contrastive-based representation learning, and to rethink the necessity of inter-modal alignment in the context of multi-modal GCD.

### 3.3. Dual-Branch Clustering

To fully discover the differences between modalities, we deploy dual-branch classifiers to tackle with image and text embeddings. The training of the two branch classifiers is conducted concurrently with the representation learning and is divided into warm-up and alignment stages.

**Warm-up Stage.** Following SimGCD [25], we adopt the loss  $\mathcal{L}_{\text{cls}}$  in Eq. (3) for training classifiers. Specifically, the

dual-branch classifiers accept image and text embeddings as the input, yielding modality-specific clustering losses  $\mathcal{L}_{\text{cls}}^I$  and  $\mathcal{L}_{\text{cls}}^T$ . By combining the representation losses in Eq. (8), the total loss during the warm-up stage becomes:

**Alignment Stage.** To align the orders of pseudo-labels predicted by dual-branch classifiers, we follow the co-teaching strategy of TextGCD [30]. By combining the loss  $\mathcal{L}_{\text{co-teach}}$  in Eq 4, the total training loss in the alignment stage is formulated as:

$$\mathcal{L}_{\text{align}} = \mathcal{L}_{\text{SSR}^2}^I + \mathcal{L}_{\text{SSR}^2}^T + \mathcal{L}_{\text{cls}}^I + \mathcal{L}_{\text{cls}}^T + \mathcal{L}_{\text{co-teach}}. \quad (10)$$

After training, the predicted pseudo-label of the  $i$ -th image is calculated by  $\arg \max(\mathbf{y}_i^I + \mathbf{y}_i^T)$ .

**Remark.** The clustering algorithm of our framework is the same as that in previous multi-modal GCD methods. However, the key distinction lies in representation learning. Specifically, TextGCD emphasizes only on the inter-modal alignment without incorporating the intra-modal constraints, and the learning of dual-branch classifiers is based on intra-modal similarities. As criticized in [11], using inter-modal alignment loss without intra-modal constraint will lead to intra-modal misalignment, i.e., the intra-modal similarities might not correspond to the actual pairwise relationships, thereby degrading the performance of intra-modal clustering. In contrast, the intra-modal relationships are well aligned by using  $\mathcal{L}_{\text{SSR}^2}$ , and thus the dual-branch classifiers produce satisfactory results. In addition, the predictions produced by the dual-branch classifiers are also utilized as self-supervised signals to guide the joint representation learning, as shown in Eq. (7).

## 4. Experiments

**Datasets.** We evaluate the performance of GCD methods on generic datasets, i.e., CIFAR-10/100 [6], and ImageNet-100/-1k [4], and fine-grained datasets, i.e., CUB-200-2011 [21], Stanford Cars [5], Oxford Pets [14] and Oxford 102 Flowers [12]. Following the GCD protocol [20], half of the samples from the known categories are selected to form the labeled dataset  $\mathcal{D}_L$ , while the remaining samples constitute the unlabeled dataset  $\mathcal{D}_U$ .

**Metrics.** Given pseudo-labels and ground-truths of  $\mathcal{D}_U$ , one can compute the clustering accuracy (ACC) using Hungarian matching algorithm [8]. Following the GCD protocol, we report ACC on all categories (“All”), on known categories (“Old”), and on unknown categories (“New”), respectively. The average ACC over 3 trials is reported.

**Implementation Details.** In Retrieval-based Text Aggregation, we use the CLIP-H/14 [15] to search prompt candidates to ensure a fair comparison to TextGCD [30]. During training, we use the CLIP-B/16 encoders to produce

Table 1. The average ACC (%) on ImageNet datasets. “†” denotes the reproduction of using CLIP backbone.

		ImageNet-100			ImageNet-1k		
Method		All	Old	New	All	Old	New
DINOv1	GCD	74.1	89.8	66.3	52.5	72.5	42.2
	SimGCD	83.0	93.1	77.9	57.1	77.3	46.9
	SPTNet	85.4	93.2	81.4	-	-	-
	SelEx	83.1	93.6	77.8	-	-	-
	Hyp-SelEx	86.8	94.6	82.8	-	-	-
	SimGCD†	86.1	94.5	81.9	48.2	72.7	36.0
CLIP	CLIP-GCD	84.0	95.5	78.2	-	-	-
	TextGCD	88.0	92.4	85.2	64.8	<b>77.8</b>	58.3
	GET	91.7	95.7	89.7	62.4	74.0	56.6
	<b>Ours</b>	<b>92.1</b>	<b>96.0</b>	<b>90.2</b>	<b>66.7</b>	77.3	<b>61.1</b>

text and image features. We report the performance of uni-modal counterparts using DINO [3] with ViT-B/16. The classifier parameters are set following the default configurations as in SimGCD [25] and TextGCD [30]. More details are provided in the supplementary.

#### 4.1. Performance on Benchmark Datasets

We compare the performance of SSR<sup>2</sup>-GCD with recent uni-modal GCD methods, including GCD [20], GPC [29], SimGCD [25], PromptCAL [28], SPTNet [23], SelEx [16] and HypCD [10] with the SelEx backbone (denoted by “Hyp-SelEx”), and multi-modal GCD methods, including CLIP-GCD [13], TextGCD [30] and GET [22]. Since that GET did not provide results on Oxford Pets and Flowers102, we reproduce the results with the open-source code. As shown in Tables 1 and 2, our method consistently outperforms all other multi-modal counterparts on all tested datasets. We can also observe that our method decreases the accuracy gap between “Old” and “New” categories, and we will discuss it in the latter section. HypCD achieves the highest accuracy on CUB when using SelEx as the backbone. HypCD changes the embedding space from the Euclidean to the hyperbolic, and thus it is complementary to our method. In addition, our method excels notably on the datasets Stanford Cars and Flowers102, achieving an accuracy of 89.2% and 93.5% on “All” categories, outperforming all other baselines by 3.1% and 6.3%, respectively. Note that CLIP performs poorly in out-of-domain datasets including Flowers102, achieving an accuracy of 70.4% in zero-shot classification [15]. Our method effectively refines the representations generated by CLIP to the target domain of Flowers102 and yields satisfactory performance.

#### 4.2. Evaluation on Representation Learning

**Naive Merging of Inter- and Intra-Modal Losses can be Ill-Advised.** To evaluate the effect of using inter-modal and intra-modal alignment in our framework, we keep the text generation and classification methods the same and re-

port the performance of using different losses for representation learning, including the inter-modal loss (i.e.,  $\mathcal{L}_{\text{CLIP}}$  in Eq. (1)), the intra-modal losses (i.e.,  $\mathcal{L}_{\text{con}}$  in Eq. (2) and our  $\mathcal{L}_{\text{SSR}^2}$  in Eq. (7)) and their combinations (e.g.,  $\mathcal{L}_{\text{CLIP}} + \mathcal{L}_{\text{con}}$ ). As can be seen in Table 3, we find that encouraging inter-modal alignment alone provides merely limited performance gain when compared to using the intra-modal losses alone, since that the learning of classifiers is based on the intra-modal relationships within each modality. Specifically, our framework achieves the highest accuracy on five benchmark datasets when using the proposed  $\mathcal{L}_{\text{SSR}^2}$ . Our framework trained with supervised and unsupervised contrastive loss  $\mathcal{L}_{\text{con}}$  is still a strong intra-modal learning baseline, achieving the highest accuracy on CIFAR-100. Interestingly, combining  $\mathcal{L}_{\text{CLIP}}$  with intra-modal losses  $\mathcal{L}_{\text{con}}$  or  $\mathcal{L}_{\text{SSR}^2}$  cannot significantly improve the clustering accuracy and even may obstacle the intra-modal learning. Specifically, “ $\mathcal{L}_{\text{con}}$ ” outperforms “ $\mathcal{L}_{\text{CLIP}} + \mathcal{L}_{\text{con}}$ ” on four datasets, except for CUB and Oxford Pets; whereas  $\mathcal{L}_{\text{SSR}^2}$  surpasses “ $\mathcal{L}_{\text{CLIP}} + \mathcal{L}_{\text{SSR}^2}$ ” on all datasets, suggesting that explicitly imposing inter-modal alignment might hinder the intra-modal representation learning.

**SSR<sup>2</sup> works well in multi-modal representation learning.** To further evaluate the role of proposed SSR<sup>2</sup> objective in inter-modal and intra-modal alignment, We also conduct experiments and display in Figure 2 the distributions of the pairwise similarity computed by image-text, image-image, and text-text pairs, obtained from our framework, when using the loss  $\mathcal{L}_{\text{SSR}^2}$  or  $\mathcal{L}_{\text{CLIP}}$  at the beginning of the training (i.e., epoch 0), the end of the warm-up (i.e., epoch 10) and the end of the training (i.e., epoch 200), respectively. Clearly, we observe from Figure 2 that the distributions of inter-modal similarities and intra-modal similarities exhibit substantial divergence at the beginning, while the distributions of image-image and text-text similarities within each modality also differ notably. When using the proposed loss  $\mathcal{L}_{\text{SSR}^2}$ , the distributions of intra-modal similarities are well aligned in the warm-up stage, and all distributions gaps almost vanish at the end of the training. Specifically, optimizing the intra-modal alignment loss (i.e.,  $\mathcal{L}_{\text{SSR}^2}$ ) alone still helps to align the distributions of image-text similarities. By contrast, using the loss  $\mathcal{L}_{\text{CLIP}}$  can help to align the distributions of image-text similarities, whereas the image-image and text-text similarities, which are critical for GCD, remain poorly aligned.

**Discussions and Evaluations.** For the reason why the intra-modal alignment loss works well in multi-modal representation learning, we account it in the implicit inter-modal alignment and the hypothesis of clustering algorithms. On the one hand, the initial textual and visual representations are well aligned by using a pretrained CLIP model to select similar pseudo text-image pairs, while further encouraging inter-modal alignment between the em-

Table 2. The average ACC (%) on generic and fine-grained datasets. “†” denotes the reproduction of using CLIP backbone.

Method	CIFAR-10			CIFAR-100			CUB			Stanford Cars			Oxford Pets			Flowers102		
	All	Old	New	All	Old	New	All	Old	New	All	Old	New	All	Old	New	All	Old	New
GCD	91.5	97.9	88.2	73.0	76.2	66.5	51.3	56.6	48.7	39.0	57.6	29.9	80.2	85.1	77.6	74.4	74.9	74.1
GPC	92.2	98.2	89.1	77.9	85.0	63.0	55.4	58.2	53.1	42.8	59.2	32.8	-	-	-	-	-	-
<i>DINOv1</i> SimGCD	97.1	95.1	98.1	80.1	81.2	77.8	60.3	65.6	57.7	53.8	71.9	45.0	87.7	85.9	88.6	71.3	80.9	66.5
PromptCAL	97.9	96.6	98.5	81.2	84.2	75.3	62.9	64.4	62.1	50.2	70.1	40.6	-	-	-	-	-	-
SPTNet	97.3	95.0	<b>98.6</b>	81.3	84.3	75.6	65.8	68.8	65.1	59.0	79.2	49.3	-	-	-	-	-	-
SelEx	95.9	98.1	94.8	82.3	85.3	76.3	73.6	75.3	<b>72.8</b>	58.5	75.6	50.3	92.5	91.9	92.8	-	-	-
Hyp-SelEx	96.7	97.6	96.3	82.4	85.1	77.0	<b>79.8</b>	<b>75.8</b>	<b>81.8</b>	62.9	80.0	54.7	-	-	-	-	-	-
<i>CLIP</i> SimGCD†	96.6	94.7	97.5	81.6	82.6	79.5	62.0	76.8	54.6	75.9	81.4	73.1	88.6	75.2	95.7	75.3	87.8	69.0
CLIP-GCD	96.6	97.2	96.4	85.2	85.0	85.6	-	-	-	62.8	77.1	55.7	70.6	88.2	62.2	76.3	88.6	70.2
TextGCD	98.2	98.0	98.6	85.7	<b>86.3</b>	84.6	76.6	<b>80.6</b>	74.7	86.1	91.8	83.9	93.7	93.2	94.0	87.2	90.7	85.4
GET	97.2	94.6	98.5	82.1	85.5	75.5	77.0	78.1	76.4	78.5	86.8	74.5	91.1	89.7	92.4	85.5	90.8	81.3
<b>Ours</b>	<b>98.5</b>	<b>98.3</b>	<b>98.6</b>	<b>86.4</b>	86.2	<b>86.9</b>	78.3	78.5	78.2	<b>89.2</b>	<b>93.1</b>	<b>87.3</b>	<b>95.7</b>	<b>95.1</b>	<b>96.0</b>	<b>93.5</b>	<b>93.3</b>	<b>93.9</b>

Table 3. Evaluation of different representation learning methods. Average ACC (%) on “All” categories is reported. “N/A” denotes using frozen CLIP.

Rep. Losses	Inter	Intra	CIFAR-10	CIFAR-100	CUB	Stanford Cars	Oxford Pets	Flowers102
N/A	×	×	97.9	84.1	74.5	86.0	91.9	87.4
$\mathcal{L}_{\text{CLIP}}$	✓	×	98.3	86.0	76.7	87.0	94.1	89.7
$\mathcal{L}_{\text{con}}$	×	✓	<u>98.4</u>	<b>86.7</b>	77.5	87.9	94.9	91.8
$\mathcal{L}_{\text{SSR}^2}$	×	✓	<b>98.5</b>	<u>86.4</u>	<b>78.3</b>	<b>89.2</b>	<b>95.7</b>	<b>93.5</b>
$\mathcal{L}_{\text{CLIP}} + \mathcal{L}_{\text{con}}$	✓	✓	98.2	86.3	<u>78.0</u>	86.7	95.0	90.9
$\mathcal{L}_{\text{CLIP}} + \mathcal{L}_{\text{SSR}^2}$	✓	✓	98.3	86.1	<u>77.2</u>	<u>88.1</u>	<u>95.0</u>	<u>92.9</u>

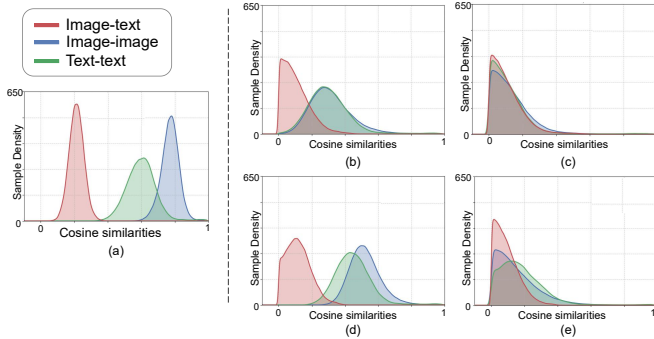


Figure 2. Distribution of pairwise similarities on the Flowers102 dataset (a): at the beginning of training, (b)-(c): training with  $\mathcal{L}_{\text{SSR}^2}$  at epochs 10 and 200, and (d)-(e): training with  $\mathcal{L}_{\text{CLIP}}$  at epochs 10 and 200.

beddings of pseudo texts and images can be noisy. Furthermore, optimizing the proposed  $\mathcal{L}_{\text{SSR}^2}$  objective does not compromise inter-modal alignment; on the contrary, as shown in Figure 2, it implicitly promotes such alignment through intra-modal mechanisms. On the other hand, most GCD frameworks, including ours, utilize a self-distillation loss for clustering. As detailed in Eq. (3), the self-distillation loss, which minimizes the cross-entropy between the predictions of augmented data pairs from the same modality, is built on the assumption that the intra-

modal embeddings of augmented data pairs should be close enough to be assigned to the same cluster. In other words, this loss rely on the hypothesis that only involves the consistency of the intra-modal embedding pairs. To quantify such intra-modal consistency, we construct the adjacency matrices  $W$  for each modality, in which the weighted edges are the cosine similarities of the intra-modal embedding pairs, i.e.,  $W_{i,j} = \mathbf{z}_i^\top \mathbf{z}_j$ . Given the ground-truth categories  $\{\mathcal{C}_1, \dots, \mathcal{C}_k\}$  indicated by their labels, one can quantize the consistency by computing the ratio of edges within each category to edges between categories, i.e.,

$$R_e = \frac{1}{k} \sum_{\ell=1}^k R_e(\mathcal{C}_\ell), \quad R_e(\mathcal{C}_\ell) = \frac{\sum_{i \in \mathcal{C}_\ell} \sum_{j \in \mathcal{C}_\ell} W_{i,j}}{\sum_{i \in \mathcal{C}_\ell} \sum_{j \notin \mathcal{C}_\ell} W_{i,j}}. \quad (11)$$

Apparently, a larger value of  $R_e$  indicates a higher ratio of correct intra-category links to incorrect inter-category links, reflecting better consistency of intra-modal embeddings.

In Figure 3 we show the  $R_e$  curves with different representation losses (i.e.,  $\mathcal{L}_{\text{CLIP}}$ ,  $\mathcal{L}_{\text{SSR}^2}$  and  $\mathcal{L}_{\text{CLIP}} + \mathcal{L}_{\text{SSR}^2}$ ) on Flowers102. As can be seen, our framework achieves higher  $R_e$  by using  $\mathcal{L}_{\text{SSR}^2}$  when compared to using  $\mathcal{L}_{\text{CLIP}}$ . While  $\mathcal{L}_{\text{CLIP}}$  can implicitly enhance intra-class discriminability to some extent, it is insufficient to ensure intra-modal alignment and thus achieves less satisfactory clustering accuracy. This verifies that the inter-modal alignment without any intra-modal constraint leads to intra-modal misalign-

ment. Moreover, we can see that the  $R_e$  curve of using  $\mathcal{L}_{\text{CLIP}} + \mathcal{L}_{\text{SSR}^2}$  rises in step with that of using  $\mathcal{L}_{\text{SSR}^2}$  early in training, eventually converges toward the curve of using  $\mathcal{L}_{\text{CLIP}}$ . This verifies that the inter-modal alignment may damage the learning of intra-modal consistency.

**SSR<sup>2</sup> is a Compressor for Balanced Representation.** To evaluate the effectiveness of our proposed  $\mathcal{L}_{\text{SSR}^2}$ , we conduct experiments to compare it to the widely used contrastive loss  $\mathcal{L}_{\text{con}}$ . To quantify the uniformity of the compression, we compute the effective rank, which is defined as the number of leading singular values whose cumulative energy proportion reaches 95% of all singular values, of image embeddings per category, i.e.,  $\{\text{rank}(\mathbf{Z}^{(i)})\}_{i=1}^k$ , where  $\mathbf{Z}^{(i)}$  is the sub-matrix formed by embeddings from  $i$ -th ground-truth category. We train our framework via using  $\mathcal{L}_{\text{con}}$  and  $\mathcal{L}_{\text{SSR}^2}$ , respectively, and plot the averaged ranks of ‘‘Old’’ categories and ‘‘New’’ categories, i.e.,  $\frac{1}{|\mathcal{Y}_l|} \sum_{i \in \mathcal{Y}_l} \text{rank}(\mathbf{Z}^{(i)})$  and  $\frac{1}{|\mathcal{Y}_u \setminus \mathcal{Y}_l|} \sum_{j \in (\mathcal{Y}_u \setminus \mathcal{Y}_l)} \text{rank}(\mathbf{Z}^{(j)})$  on Flowers102 and Oxford Pets, respectively, and display the results in Figure 4. We can see that the average rank of the ‘‘Old’’ categories dramatically decreases during the training period when using the loss  $\mathcal{L}_{\text{con}}$ , which is much lower than that of the ‘‘New’’ categories. Intuitively, using the loss  $\mathcal{L}_{\text{con}}$  will overly compress the embeddings toward the contrastive prototypes of the known categories, and thereby damages the accuracy of clustering those data points in the boundaries of the category manifolds. In contrast, when training with the loss  $\mathcal{L}_{\text{SSR}^2}$ , the average ranks of the ‘‘Old’’ and ‘‘New’’ categories are preserved well. This indicates that the embeddings of each category are compressed evenly, resulting in comparable clustering accuracy of ‘‘Old’’ and ‘‘New’’ categories (see, e.g., Table 2).

To have a better intuition, we use  $t$ -SNE [18] to visualize the image embeddings produced by using frozen CLIP encoder, optimizing  $\mathcal{L}_{\text{CLIP}}$ , optimizing  $\mathcal{L}_{\text{con}}$  and our approach. We display the experimental results on CIFAR-10 in Figure 5. Clearly, we observe that our approach learns well-aligned and well-balanced representations that are evenly compressed within categories and discriminative between categories.

### 4.3. Ablation Study

To evaluate the effectiveness of each component in the proposed approach, we conduct a set of experiments on Stanford Cars and Flowers-102, in which the baseline is set up by using the most similar tag as pseudo-text, leveraging the frozen CLIP to generate embeddings, and clustering both image and text embeddings with shared parameters of a single classifier. Experimental results are listed in Table 4. We can read that the co-taught dual-branch classifiers outperform the baseline by identifying disparities between modalities. The proposed RTA integrates rich information from

tag and attribute candidates, thereby enhancing clustering performance on ‘‘New’’ categories. The intra-modal representation learning with using the loss  $\mathcal{L}_{\text{SSR}^2}$  is also critical, as the training of classifiers relies on intra-modal relationships. Our framework achieves best performance by integrating all proposed components.

Table 4. Ablation study of different components.

Dual	RTA	$\mathcal{L}_{\text{SSR}^2}$	Stanford Cars			Flowers102		
			All	Old	New	All	Old	New
×	×	×	75.2	85.4	71.8	78.3	88.1	72.5
✓	×	×	81.7	90.3	77.1	83.9	88.3	81.3
✓	✓	×	86.0	91.0	83.4	87.4	90.8	85.5
✓	×	✓	85.5	91.7	82.2	89.1	91.8	88.0
✓	✓	✓	<b>89.2</b>	<b>93.1</b>	<b>87.3</b>	<b>93.5</b>	<b>93.3</b>	<b>93.9</b>

### 4.4. More Evaluations

**Evaluation on Retrieval-based Text Aggregation.** In our proposed Retrieval-based Text Aggregation (RTA), the hyper-parameter  $\alpha$  serves as the balance factor of integrating most-similar candidates and other candidates. To evaluate the effect of hyper-parameter  $\alpha$ , we report the accuracy of ‘‘All’’ categories on 4 generic and fine-grained datasets, with varying values of  $\alpha$  in  $\{0.2, 0.3, 0.4, 0.5, 0.6, 0.7, 0.8\}$  while keeping other components in our framework unchanged. As shown in Table 5, we observe that using the proposed RTA achieves its best performance on CIFAR-10, Stanford Cars and Flowers102 with  $\alpha = 0.5$ , and achieves its best performance on CIFAR-100 with  $\alpha = 0.4$ .

In RTA, we select multiple candidates for tags and attributes. To evaluate the effect of the number of candidates, we report the accuracy of ‘‘All’’ categories on the four generic and fine-grained datasets, with varying number of tags and attributes in  $\{1, 2, 3, 4, 5\}$ , respectively, while keeping other components in our framework unchanged. As shown in Figure 6, we can read that integrating more information from candidates yields consistent performance improvements. Specifically, the proposed RTA achieves its best performance when the number of candidates for tags and attributes is set to 3 or 4, respectively.

Table 5. Effect of the hyper-parameter  $\alpha$  in RTA strategy.

Data	$\alpha$	0.2	0.3	0.4	0.5	0.6	0.7	0.8
CIFAR-10		98.3	98.4	98.4	<b>98.5</b>	98.3	98.2	97.8
CIFAR-100		86.0	86.6	<b>86.7</b>	86.4	85.8	85.2	84.1
Stanford Cars		87.1	88.7	88.9	<b>89.2</b>	88.8	87.2	86.4
Flowers102		92.9	93.3	93.3	<b>93.5</b>	92.8	92.1	91.5

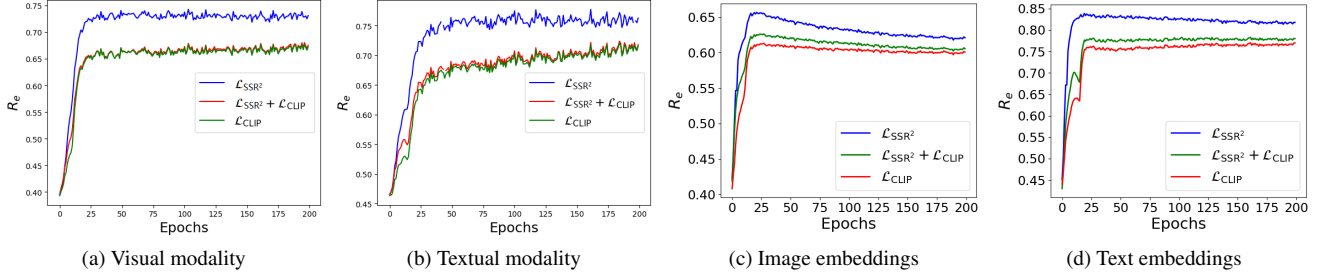


Figure 3.  $R_e$  curves with different losses on (a)-(b): Flowers102 and (c)-(d): Stanford Cars datasets.

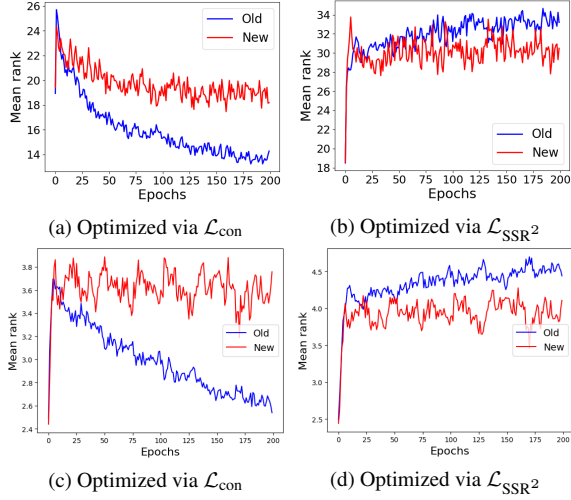


Figure 4. Effective ranks of image embeddings in (a)-(b): Oxford Pets, and (c)-(d): Flowers102 datasets.

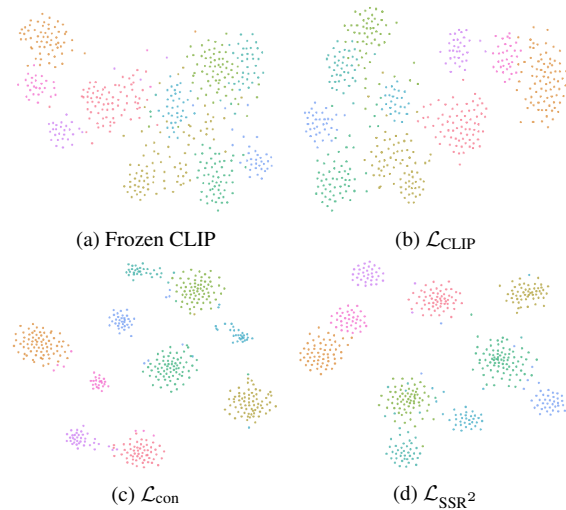


Figure 5. Visualizations of image embeddings via different representation learning methods.

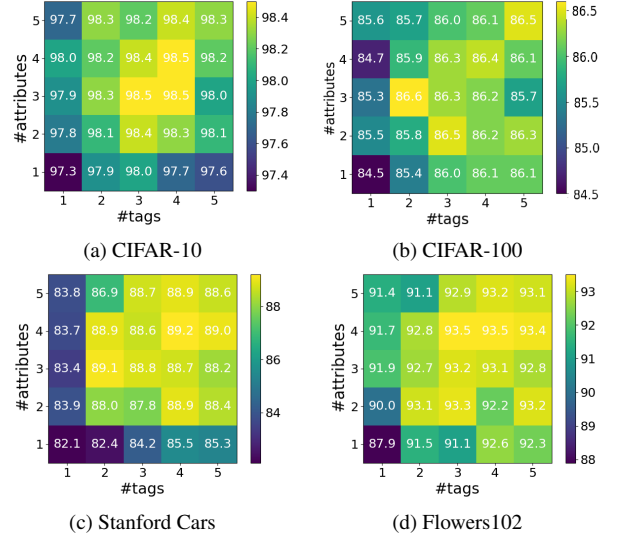


Figure 6. Effect of the number of candidates.

## 5. Conclusion

We have proposed a novel and effective framework, called  $SSR^2$ -GCD, to tackle with the multi-modal GCD task. In particular, we incorporated a semi-supervised rate reduction loss to learn structured representations that are evenly compressed across categories. Moreover, we have presented a retrieval-based text aggregation approach to enhance text generation to boost knowledge transfer. We have conducted extensive experiments on eight benchmark datasets and experimental results have verified our findings and demonstrated the effectiveness of our proposed  $SSR^2$ -GCD approach.

**Limitations.** We note that the time and memory burden of our approach will slightly increase when the number of candidates is enlarged due to using multiple tag and attribute candidates as the input to CLIP encoders. Besides, in our current framework, the image and text cues are treated equally. A further exploration on the importance of each modality in the multi-modal GCD task is left for future work.

## References

- [1] Mahmoud Assran, Mathilde Caron, Ishan Misra, Piotr Bojanowski, Florian Bordes, Pascal Vincent, Armand Joulin, Mike Rabbat, and Nicolas Ballas. Masked siamese networks for label-efficient learning. In *European Conference on Computer Vision*, pages 456–473, 2022. 2
- [2] Tom B. Brown, Benjamin Mann, Nick Ryder, Melanie Subbiah, Jared Kaplan, Prafulla Dhariwal, Arvind Neelakantan, Pranav Shyam, Girish Sastry, Amanda Askell, Sandhini Agarwal, Ariel Herbert-Voss, Gretchen Krueger, Tom Henighan, Rewon Child, Aditya Ramesh, Daniel M. Ziegler, Jeffrey Wu, Clemens Winter, Christopher Hesse, Mark Chen, Eric Sigler, Mateusz Litwin, Scott Gray, Benjamin Chess, Jack Clark, Christopher Berner, Sam McCandlish, Alec Radford, Ilya Sutskever, and Dario Amodei. Language models are few-shot learners. In *Advances in Neural Information Processing Systems*, 2020. 2
- [3] Mathilde Caron, Hugo Touvron, Ishan Misra, Hervé Jégou, Julien Mairal, Piotr Bojanowski, and Armand Joulin. Emerging properties in self-supervised vision transformers. In *IEEE/CVF International Conference on Computer Vision*, pages 9630–9640. IEEE, 2021. 5
- [4] Jia Deng, Wei Dong, Richard Socher, Li-Jia Li, Kai Li, and Li Fei-Fei. Imagenet: A large-scale hierarchical image database. In *IEEE conference on computer vision and pattern recognition*, pages 248–255, 2009. 2, 4
- [5] Jonathan Krause, Michael Stark, Jia Deng, and Li Fei-Fei. 3d object representations for fine-grained categorization. In *Proceedings of the IEEE international conference on computer vision workshops*, pages 554–561, 2013. 4
- [6] Alex Krizhevsky, Geoffrey Hinton, et al. Learning multiple layers of features from tiny images. *Technical Report TR-2009, University of Toronto, Toronto*, 2009. 4
- [7] A. Krizhevsky, I. Sutskever, and G. Hinton. Imagenet classification with deep convolutional neural networks. In *Advances in Neural Information Processing Systems*, pages 1097–1105, 2012. 2
- [8] Harold W. Kuhn. The hungarian method for the assignment problem. *Naval research logistics quarterly*, 2(1-2):83–97, 1955. 4
- [9] Yunfan Li, Peng Hu, Dezhong Peng, Jiancheng Lv, Jianping Fan, and Xi Peng. Image clustering with external guidance. In *International Conference on Machine Learning*, 2024. 2
- [10] Yuanpei Liu, Zhenqi He, and Kai Han. Hyperbolic category discovery. In *Proceedings of the IEEE/CVF Conference on Computer Vision and Pattern Recognition*, 2025. 5
- [11] Marco Mistretta, Alberto Baldrati, Lorenzo Agnolucci, Marco Bertini, and Andrew D. Bagdanov. Cross the gap: Exposing the intra-modal misalignment in clip via modality inversion. In *Proceedings of the International Conference on Learning Representations*, 2025. 4
- [12] Maria-Elena Nilsback and Andrew Zisserman. Automated flower classification over a large number of classes. In *Sixth Indian Conference on Computer Vision, Graphics & Image Processing*, pages 722–729. IEEE Computer Society, 2008. 4
- [13] Rabah Ouldoughi, Chia-Wen Kuo, and Zsolt Kira. Clipgcd: Simple language guided generalized category discovery, 2023. 1, 5
- [14] Omkar M Parkhi, Andrea Vedaldi, Andrew Zisserman, and C V Jawahar. Cats and dogs. In *Proceedings of the IEEE/CVF Conference on Computer Vision and Pattern Recognition*, pages 3498–3505. IEEE, 2012. 4
- [15] Alec Radford, Jong Wook Kim, Chris Hallacy, Aditya Ramesh, Gabriel Goh, Sandhini Agarwal, Girish Sastry, Amanda Askell, Pamela Mishkin, Jack Clark, Gretchen Krueger, and Ilya Sutskever. Learning transferable visual models from natural language supervision. In *International Conference on Machine Learning*, pages 8748–8763. PMLR, 2021. 1, 4, 5, 13
- [16] Sarah Rastegar, Mohammadreza Salehi, Yuki M Asano, Hazel Doughty, and Cees GM Snoek. Selex: Self-expertise in fine-grained generalized category discovery. In *European Conference on Computer Vision*, pages 440–458, 2024. 5
- [17] Walter J Scheirer, Anderson de Rezende Rocha, Archana Sapkota, and Terrance E Boulton. Toward open set recognition. *IEEE transactions on pattern analysis and machine intelligence*, 35(7):1757–1772, 2012. 1
- [18] Laurens Van der Maaten and Geoffrey Hinton. Visualizing data using t-sne. *Journal of machine learning research*, 9(11), 2008. 7
- [19] Wouter Van Gansbeke, Simon Vandenhende, Stamatios Georgoulis, Marc Proesmans, and Luc Van Gool. Scan: Learning to classify images without labels. In *European Conference on Computer Vision*, pages 268–285, 2020. 3
- [20] Sagar Vaze, Kai Hant, Andrea Vedaldi, and Andrew Zisserman. Generalized category discovery. In *Proceedings of the IEEE/CVF Conference on Computer Vision and Pattern Recognition*, pages 7482–7491, 2022. 1, 4, 5
- [21] C. Wah, S. Branson, P. Welinder, P. Perona, and S. Belongie. The caltech-ucsd birds-200-2011 dataset. Technical Report CNS-TR-2011-001, California Institute of Technology, 2011. 4
- [22] Enguang Wang, Zhimao Peng, Zhengyuan Xie, Fei Yang, Xialei Liu, and Ming-Ming Cheng. Get: Unlocking the multi-modal potential of clip for generalized category discovery. In *Proceedings of the IEEE/CVF Conference on Computer Vision and Pattern Recognition*, pages 20296–20306, 2025. 1, 2, 5
- [23] Hongjun Wang, Sagar Vaze, and Kai Han. Sptnet: An efficient alternative framework for generalized category discovery with spatial prompt tuning. In *International Conference on Learning Representations*, 2024. 5
- [24] Peng Wang, Huikang Liu, Druv Pai, Yaodong Yu, Zhihui Zhu, Qing Qu, and Yi Ma. A global geometric analysis of maximal coding rate reduction. In *International Conference on Machine Learning*, 2024, 2024. 4
- [25] Xin Wen, Bingchen Zhao, and Xiaojuan Qi. Parametric classification for generalized category discovery: A baseline study. In *Proceedings of the IEEE International Conference on Computer Vision*, pages 16544–16554, 2023. 2, 4, 5
- [26] Yaodong Yu, Kwan Ho Ryan Chan, Chong You, Chaobing Song, and Yi Ma. Learning diverse and discriminative rep-

- representations via the principle of maximal coding rate reduction. In *Advances in Neural Information Processing Systems*, pages 9422–9434, 2020. [1](#), [3](#), [4](#)
- [27] Beichen Zhang, Pan Zhang, Xiaoyi Dong, Yuhang Zang, and Jiaqi Wang. Long-clip: Unlocking the long-text capability of clip. In *European Conference on Computer Vision*, pages 310–325, 2024. [3](#)
- [28] Sheng Zhang, Salman Khan, Zhiqiang Shen, Muzammal Naseer, Guangyi Chen, and Fahad Shahbaz Khan. Prompt-cal: Contrastive affinity learning via auxiliary prompts for generalized novel category discovery. In *Proceedings of the IEEE/CVF Conference on Computer Vision and Pattern Recognition*, pages 3479–3488, 2023. [5](#)
- [29] Bingchen Zhao, Xin Wen, and Kai Han. Learning semi-supervised gaussian mixture models for generalized category discovery. In *Proceedings of the IEEE International Conference on Computer Vision*, pages 16577–16587, 2023. [5](#)
- [30] Haiyang Zheng, Nan Pu, Wenjing Li, Nicu Sebe, and Zhun Zhong. Textual knowledge matters: Cross-modality co-teaching for generalized visual class discovery. In *European Conference on Computer Vision*, pages 41–58, 2025. [1](#), [2](#), [3](#), [4](#), [5](#), [12](#)

## A. Experimental Details

### A.1. Datasets

In Table A.1, we provide a statistical summarization of all generic and fine-grained datasets. Among these benchmarks, the generic datasets including CIFAR-10, CIFAR-100, ImageNet-100 and ImageNet-1k consist of categories of open-world, whereas the fine-grained benchmarks including CUB, Stanford Cars, Oxford Pets, and Flowers102 are largely domain-specific. Following the GCD protocol, we select the first 80 classes of CIFAR-100 as the known categories and use the first half of classes as the known categories for the other benchmarks.

Table A.1. Statistics of the benchmark datasets.

Dataset	Labelled		Unlabelled	
	#Image	#Class	#Image	#Class
CIFAR10	12.5K	5	37.5K	10
CIFAR100	20.0K	80	30.0K	100
ImageNet-100	31.9K	50	95.3K	100
ImageNet-1K	321K	500	960K	1000
CUB	1.5K	100	4.5K	200
Stanford Cars	2.0K	98	6.1K	196
Oxford Pets	1.9K	19	5.5K	37
Flowers102	0.3K	51	0.8K	102

### A.2. Experiment Settings

**Model Architecture.** In Figure A.1, we present an detailed overview of proposed Retrieval-based Text Aggregation (RTA). In Table A.2, we present the model architecture of the learnable parameters in the CLIP encoders and classifiers. The visual and textual branches share the same model architecture. Specifically, when using CLIP-B/16 as the backbone, we fine-tune the last residual attention block (which includes the multi-head self-attention mechanism, feed-forward network, and layer normalization), along with the image and text projectors of CLIP. Additionally, the dual-branch classifiers are learned with the fine-tuning of CLIP jointly.

**Data Preparation.** For each mini-batch data, we generate text embeddings for query images by integrating 4 similar

Table A.2. Model architectures. “CLIP” denotes the learnable parameters in CLIP and “Cls” denotes the classifiers.

CLIP	Last residual attention block: $\mathbb{R}^{512} \rightarrow \mathbb{R}^{512}$
	Image/text projector: $\mathbb{R}^{512} \rightarrow \mathbb{R}^{512}$
Cls.	Linear: $\mathbb{R}^{512} \rightarrow \mathbb{R}^k$
	Softmax

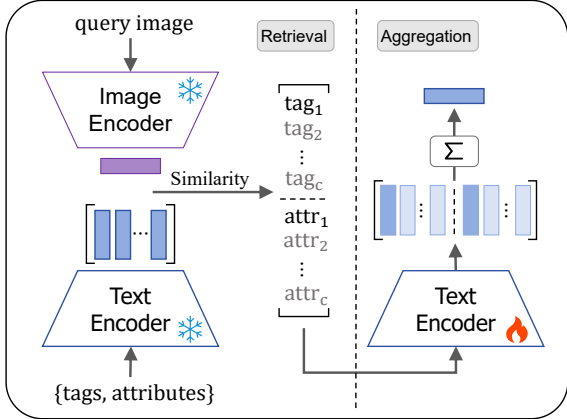


Figure A.1. An overview of Retrieval-based Text Aggregation.

Table A.3. Pseudo-code of the image augmentation.

```

from torchvision.transforms import *

Compose ([
    RandomResizedCrop(32, BILINEAR)
    RandomHorizontalFlip(p=0.5),
    ColorJitter()
    ToTensor(),
    Normalize([0.485, 0.456, 0.406],
              [0.229, 0.224, 0.225])
])

```

Table A.4. Pseudo-code of the text augmentation.

**Text Augmentation Strategy**

**Input:** text

**For each word in text:**

**If** len(word) ≥ 3:

        index ← random(1, len(word)-2)

        action ← random( {replace, delete, add, none} )

**Case action:**

            replace: word ← replace random char at index

            delete: word ← remove char at index

            add: word ← insert random char at index

            none: **continue**

**Output:** augmented text

tags and 4 similar attributes through the proposed retrieval-based text aggregation by using the encoders of CLIP-H/14 for all tested datasets. Then, both images and text are augmented into two views, and the augmentation strategies are the same across datasets, as detailed in Tables A.3 and A.4. The embeddings of augmented images and text are used for representation learning.

**Training Settings.** We use the same setting for all tested datasets. We use the the stochastic gradient descent (SGD) with the momentum of 0.9, the weight decay of  $1 \times 10^{-4}$ , and the cosine annealing learning rate decay for the training process. We train the model for 200 epochs and set

Table A.5. The mean  $\pm$  std ACC (%) of TextGCD, GET and our approach on generic datasets.

Method	CIFAR-10			CIFAR-100			ImageNet-100			ImageNet-1k		
	All	Old	New									
TextGCD	98.2 $\pm$ 0.0	98.0 $\pm$ 0.2	<b>98.6</b> $\pm$ 0.1	85.7 $\pm$ 0.9	<b>86.3</b> $\pm$ 0.6	84.6 $\pm$ 2.2	88.0 $\pm$ 0.6	92.4 $\pm$ 0.9	85.2 $\pm$ 1.2	64.8 $\pm$ 0.2	<b>77.8</b> $\pm$ 0.5	58.3 $\pm$ 0.4
GET	97.2 $\pm$ 0.1	94.6 $\pm$ 0.1	98.5 $\pm$ 0.1	82.1 $\pm$ 0.4	85.5 $\pm$ 0.5	75.5 $\pm$ 0.5	91.7 $\pm$ 0.3	95.7 $\pm$ 0.0	89.7 $\pm$ 0.4	62.4 $\pm$ 0.0	74.0 $\pm$ 0.2	56.6 $\pm$ 0.1
<b>Ours</b>	<b>98.5</b> $\pm$ 0.2	<b>98.3</b> $\pm$ 0.2	<b>98.6</b> $\pm$ 0.3	<b>86.4</b> $\pm$ 0.5	86.2 $\pm$ 0.6	<b>86.9</b> $\pm$ 1.6	<b>92.1</b> $\pm$ 0.3	<b>96.0</b> $\pm$ 0.6	<b>90.2</b> $\pm$ 0.8	<b>66.7</b> $\pm$ 0.1	77.3 $\pm$ 0.3	<b>61.1</b> $\pm$ 0.2

Table A.6. The mean  $\pm$  std ACC (%) of TextGCD, GET and our approach on fine-grained datasets.

Method	CUB			Stanford Cars			Oxford Pets			Flowers102		
	All	Old	New									
TextGCD	76.6 $\pm$ 0.6	<b>80.6</b> $\pm$ 2.0	74.7 $\pm$ 1.7	86.1 $\pm$ 0.9	91.8 $\pm$ 0.4	83.9 $\pm$ 1.3	93.7 $\pm$ 0.6	93.2 $\pm$ 1.1	94.0 $\pm$ 0.9	87.2 $\pm$ 2.3	90.7 $\pm$ 1.3	85.4 $\pm$ 3.8
GET	77.0 $\pm$ 0.5	78.1 $\pm$ 1.6	76.4 $\pm$ 1.2	78.5 $\pm$ 1.3	86.8 $\pm$ 1.5	74.5 $\pm$ 2.2	91.1 $\pm$ 1.0	89.7 $\pm$ 1.6	92.4 $\pm$ 1.2	85.5 $\pm$ 0.5	90.8 $\pm$ 1.5	81.3 $\pm$ 1.7
<b>Ours</b>	<b>78.3</b> $\pm$ 0.8	78.5 $\pm$ 1.2	<b>78.2</b> $\pm$ 0.9	<b>89.2</b> $\pm$ 0.3	<b>93.1</b> $\pm$ 0.9	<b>87.3</b> $\pm$ 0.2	<b>95.7</b> $\pm$ 0.2	<b>95.1</b> $\pm$ 0.5	<b>96.0</b> $\pm$ 0.4	<b>93.5</b> $\pm$ 0.4	<b>93.3</b> $\pm$ 0.8	<b>93.9</b> $\pm$ 1.0

the batch size to 128. The random seed for 3-trials is set to  $[0, 1, 2]$ . For representation learning, the initial learning rate for CLIP is set to 0.001, and our proposed objective  $\mathcal{L}_{SSR^2}$  does not introduce an additional hyper-parameter. For clustering, the setting follows the default configurations as in SimGCD and TextGCD. Specifically, the initial learning rate for classifiers is set to 0.1, the epochs for warm-up stage is set to 10, and 60% of pseudo-labels of each categories are selected for co-teaching. All experiments are conducted on single NVIDIA GeForce RTX3090 GPU.

## B. More Experiments

### B.1. Evaluation on Model Stability

In Tables A.5 and A.6, we report the mean and standard deviation of accuracies over 3 trials across tested datasets, and compare them to those of the multi-modal counterparts TextGCD and GET. As can be seen, the performance of our proposed method is relatively stable.

### B.2. Effect of Retrieval-based Text Aggregation

We report the results of  $SSR^2$ -GCD compared to TextGCD when removing prompts of *unknown* categories for each dataset from the candidate pool, since the prompts in candidate pool may semantically identical to the unknown categories. As can be seen in Table B.7, though the performance of both methods is slightly dropped, our  $SSR^2$ -GCD is still leading. For a fair comparison to other retrieval based methods, we use same candidate pool and backbones as in TextGCD to search prompt candidates in the main manuscript.

### B.3. Evaluation on Representation Learning

**Performance of  $SSR^2$  on Imbalanced Categories.** To evaluate the performance of  $SSR^2$ -GCD on imbalanced

Table B.7. Effect of retrieval-based methods with or without (w/o) prompts from unknown categories in 4 tested datasets.

Datasets	CUB	Cars	Pets	Flowers
TextGCD[30]	76.6	86.1	93.7	87.2
TextGCD (w/o)	75.7	85.5	91.5	84.0
<b><math>SSR^2</math>-GCD (w/o)</b>	<b>77.6</b>	<b>88.1</b>	<b>94.0</b>	<b>91.6</b>

datasets, we trained  $SSR^2$  on *entire* Flowers102 (class-imbalanced) dataset and visualized the cosine similarity (ordered by ground-truths) and *effective ranks* of learned features in Figure B.4.

As can be seen, showing that larger block (categories) tends to have higher rank. This is because, with the scaled compression term in  $SSR^2$  objectives, the  $SSR^2$ -GCD tends to learn “balanced” embeddings, in which bigger classes span higher ranks with smaller singular values, smaller classes span lower ranks with larger singular values, and the nonzero singular values within each class are of equal amplitude.

### Evaluation on More Inter-Modal Alignment Methods.

To further evaluate the necessity of inter-modal alignment, we report the performance of using different inter-modal representation loss for training our framework. Specifically, we reproduce the cross-modal instance consistency objective (CICO) which is proposed in GET to serve as the inter-modal alignment constraint:

$$\mathcal{L}_{CICO} = \frac{1}{2|B|} \sum_{i \in B} (D_{KL}(s_i^T || s_i^I) + D_{KL}(s_i^I || s_i^T)), \quad (12)$$

where  $D_{KL}$  is the Kullback-Leibler divergence,  $B$  denotes the mini-batch data,  $s_i^I = \text{Softmax}(z_i^T \mathcal{A}^I)$  and  $s_i^T = \text{Softmax}(z_i^T \mathcal{A}^T)$  measure the distance between the  $i$ -th image/text embeddings and prototypes, and  $\mathcal{A}^I, \mathcal{A}^T$  are the

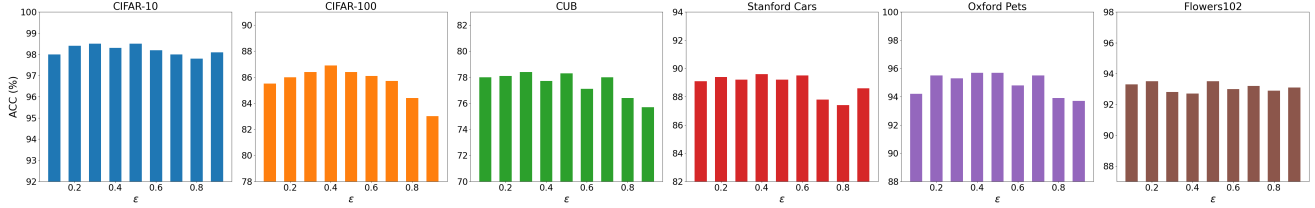


Figure A.2. ACC (%) with varying  $\epsilon$  in  $\text{SSR}^2$  across six benchmark datasets.

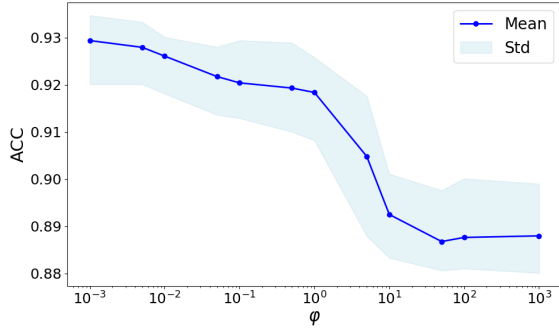


Figure B.3. Mean and standard accuracy (3 trials) of “All” categories with varying penalty weight  $\varphi$  on Flowers102.

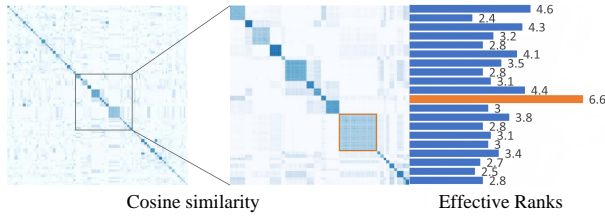


Figure B.4. Cosine similarity (ordered by GT) and cluster ranks.

prototypes calculated using the labeled anchors for each modality.

In Table B.8, we report the performance of using  $\mathcal{L}_{\text{CICO}}$  and its combination with the intra-modal alignment losses for representation learning, in which the results are marked in gray. As can be seen that, both inter-modal alignment losses  $\mathcal{L}_{\text{CLIP}}$  and  $\mathcal{L}_{\text{CICO}}$  fail to provide performance improvements when combined with the intra-modal alignment loss, further verifying the argument that the inter-modal alignment is not necessary.

To further verify that cross-modal alignment may not be necessary, and joint optimization of cross-modal alignment and intra-modal alignment significantly impairs feature learning, we validate the role of inter-modal alignment under different text prompt qualities (noise levels). Specifically, in the RTA strategy, we employ three frozen CLIP models [15], namely CLIP-H/14, CLIP-L/14, and CLIP-B/16, to conduct prompt searching, simulating the impact of cross-modal alignment on model performance under vary-

Table B.8. Evaluation of different representation learning methods. Average ACC (%) on “All” categories is reported. “N/A” denotes using frozen CLIP.

Rep. Losses	Inter	Intra	C-10	C-100	CUB	Cars	Pets	Flowers
N/A	×	×	97.9	84.1	74.5	86.0	91.9	87.4
$\mathcal{L}_{\text{CLIP}}$	✓	×	98.3	86.0	76.6	86.7	93.9	89.7
$\mathcal{L}_{\text{CICO}}$	✓	×	98.0	85.0	76.4	86.1	94.9	87.2
$\mathcal{L}_{\text{con}}$	×	✓	98.4	<b>86.7</b>	77.5	87.9	94.9	91.8
$\mathcal{L}_{\text{SSR}^2}$	×	✓	<b>98.5</b>	<b>86.4</b>	<b>78.3</b>	<b>89.2</b>	<b>95.7</b>	<b>93.5</b>
$\mathcal{L}_{\text{CLIP}}+\mathcal{L}_{\text{con}}$	✓	✓	98.2	86.3	78.0	86.7	95.0	90.9
$\mathcal{L}_{\text{CICO}}+\mathcal{L}_{\text{con}}$	✓	✓	98.4	85.9	76.8	87.0	94.4	88.6
$\mathcal{L}_{\text{CLIP}}+\mathcal{L}_{\text{SSR}^2}$	✓	✓	98.3	86.1	77.2	<u>88.1</u>	95.0	<u>92.9</u>
$\mathcal{L}_{\text{CICO}}+\mathcal{L}_{\text{SSR}^2}$	✓	✓	98.3	86.1	76.7	87.5	<u>95.5</u>	92.1

ing prompt qualities. The results in Table B.9 demonstrate that, on the Stanford Cars and Flowers102 datasets, introducing the additional  $\mathcal{L}_{\text{CLIP}}$  loss for joint training with  $\mathcal{L}_{\text{SSR}^2}$  consistently degrades clustering performance across all prompt quality levels.

**Evaluation on Uni-Modal Representation Learning.** As an intra-modal alignment loss, the proposed  $\mathcal{L}_{\text{SSR}^2}$  can also be used for uni-modal GCD counterparts. Specifically, for GCD and simGCD frameworks, we keep their pre-trained models and clustering algorithms and replace the supervised and unsupervised contrastive loss  $\mathcal{L}_{\text{con}}$  with our proposed  $\mathcal{L}_{\text{SSR}^2}$ . As can be seen from Table B.10 that, using our  $\mathcal{L}_{\text{SSR}^2}$  for representation learning achieves improvements on all tested datasets, while achieves a relatively less significant improvement on the CUB dataset.

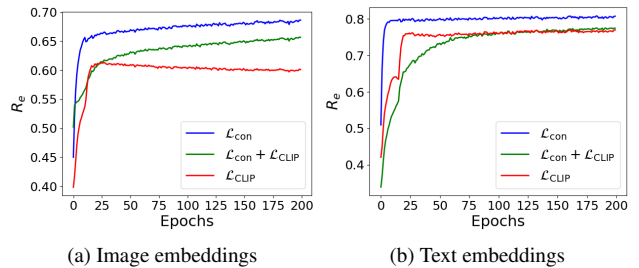


Figure B.5.  $R_e$  curves with different losses on Stanford Cars.

## Evaluation on the Role of Inter-Modal and Intra-Modal

Table B.9. Accuracy comparison of models using different feature learning methods under various text prompt qualities.  $\Delta$  denotes the accuracy difference before and after adding the cross-modal alignment loss  $\mathcal{L}_{\text{CLIP}}$ , and the arrow “ $\downarrow$ ” indicates accuracy drop.

Text Retrieval Model	Prompt Quality	Stanford Cars			Flowers102		
		$\mathcal{L}_{\text{SSR}^2}$	$\mathcal{L}_{\text{SSR}^2} + \mathcal{L}_{\text{CLIP}}$	$\Delta$	$\mathcal{L}_{\text{SSR}^2}$	$\mathcal{L}_{\text{SSR}^2} + \mathcal{L}_{\text{CLIP}}$	$\Delta$
CLIP-H/14	High	89.2	88.1	1.1 $\downarrow$	93.5	92.9	0.6 $\downarrow$
CLIP-L/14	Medium	87.5	86.1	1.4 $\downarrow$	92.4	91.8	0.6 $\downarrow$
CLIP-B/16	Low	85.2	84.0	1.2 $\downarrow$	90.1	89.8	0.3 $\downarrow$

Table B.10. Comparison to uni-modal counterparts. Clustering ACC (%) on generic and fine-grained datasets.

Method	CIFAR-10			CIFAR-100			CUB			Stanford Cars			Oxford Pets			Flowers102		
	All	Old	New	All	Old	New	All	Old	New	All	Old	New	All	Old	New	All	Old	New
GCD	91.5	<b>97.9</b>	88.2	73.0	76.2	66.5	51.3	56.6	48.7	39.0	57.6	29.9	80.2	85.1	77.6	74.4	74.9	74.1
GCD+SSR <sup>2</sup>	92.5	96.4	91.6	73.9	79.0	63.2	51.9	55.0	47.1	47.9	56.1	47.3	83.6	87.7	79.8	80.0	83.3	78.5
SimGCD	97.1	95.1	<b>98.1</b>	80.1	81.2	77.8	60.3	<b>65.6</b>	57.7	53.8	<b>71.9</b>	45.0	87.7	85.9	88.6	71.3	80.9	66.5
SimGCD+SSR <sup>2</sup>	<b>97.6</b>	97.5	97.7	<b>81.1</b>	<b>82.5</b>	<b>78.9</b>	<b>60.8</b>	64.7	<b>59.0</b>	<b>57.1</b>	66.8	<b>53.9</b>	<b>90.0</b>	<b>89.8</b>	<b>91.2</b>	<b>81.6</b>	<b>83.5</b>	<b>80.1</b>

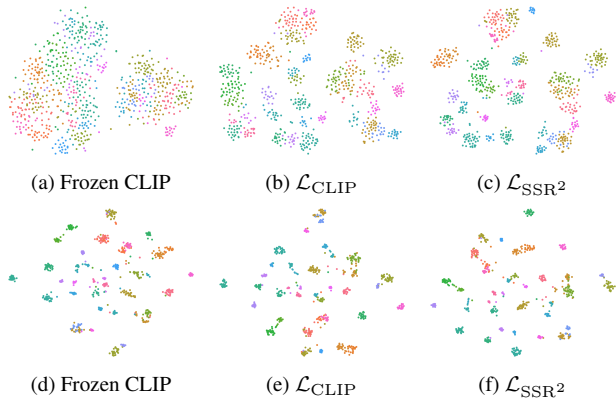


Figure B.6. Visualization of image embeddings (**top**) and text embeddings (**bottom**) on the Oxford Pets dataset.

**Alignments.** Evaluate the role of inter-modal and intra-modal interactions, we combine our proposed intra-modal alignment loss  $\mathcal{L}_{\text{SSR}^2}$  with the inter-modal alignment loss  $\mathcal{L}_{\text{CLIP}}$  by:

$$\mathcal{L}_{\text{SSR}^2} + \varphi \cdot \mathcal{L}_{\text{CLIP}},$$

where  $\varphi$  is the penalty weight of  $\mathcal{L}_{\text{CLIP}}$ . In Figure B.3, we report the accuracy with varying penalty weight  $\varphi$  on the Flowers102 dataset. Existing multi-modal GCD frameworks, such as GET, assume that the learning of inter-modal alignment does not affect that of intra-modal alignment, and naively treat these two learning processes in representation learning as both independent and equally important. However, we can see from Figure B.3 that the learning of inter-modal alignment significantly impairs the learning of intra-modal alignment as  $\varphi$  increases.

**More Results on the Ratio of Edges.** Recall that we define

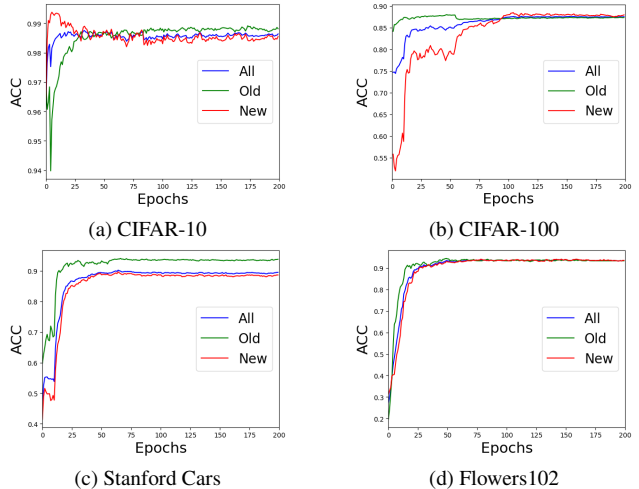


Figure B.7. ACC curves on benchmark datasets.

the ratio of edges  $R_e$  in our manuscript to quantify the intra-modal consistency of embeddings and explain why inter-modal alignment can be unnecessary. In this paragraph, we additionally report  $R_e$  of inter-modal alignment loss (i.e.,  $\mathcal{L}_{\text{CLIP}}$ ), intra-modal alignment losses (i.e.,  $\mathcal{L}_{\text{con}}$ ) and their combinations (i.e.,  $\mathcal{L}_{\text{con}} + \mathcal{L}_{\text{CLIP}}$ ) on the Stanford Cars dataset. As shown in Figure B.5, the inter-modal alignment also damages the learning of other intra-modal losses such as the widely adopted supervised and unsupervised contrastive loss  $\mathcal{L}_{\text{con}}$ . This confirms that the aforementioned trend is not exclusive to scenarios where  $\mathcal{L}_{\text{CLIP}}$  is combined with our proposed  $\mathcal{L}_{\text{SSR}^2}$ .

Table B.11. Running time and memory costs on Flowers102. † denotes Adopting the method in TextGCD to produce text features.

Methods	Running Time (sec/iter)			Memory (MB)	
	Forward	Backward	Overall	w/o RTA†	w/ RTA
TextGCD	0.34	$6.7 \times 10^{-3}$	0.69	7,622	-
SSR <sup>2</sup> -GCD	0.57	$7.5 \times 10^{-2}$	0.92	8,035	11,080

#### B.4. Evaluation on the Parameter $\epsilon$

We evaluate the impact of different hyper-parameters introduced by our representation learning method. Recall that the scaling parameter  $\epsilon > 0$  is specific to our method, while the settings of all other hyper-parameters follow those of existing GCD counterparts. In Figure A.2, we report the clustering accuracy with varying value of  $\epsilon$  on six benchmark datasets, i.e., CIFAR-10, CIFAR-100, CUB, Stanford Cars, Oxford Pets and Flowers102. As can be seen, our framework is not sensitive to  $\epsilon$  and achieves the best performance when  $\epsilon$  is in the range of [0.2, 0.5].

#### B.5. Visualization

In Figure B.6, we use  $t$ -SNE to visualize the image embeddings and text embeddings of our framework using different representation learning methods on the Oxford Pet dataset. As can be seen, the distribution of image embeddings generated by the frozen CLIP image encoder is rather diffuse and can be roughly divided into two hyper-classes (“cat” and “dog”). In contrast, thanks to our proposed Retrieval-based Text Aggregation (RTA) strategy, the distribution of text embeddings produced by the frozen CLIP text encoder exhibits significantly greater discriminability. Such discrepancies between the two modalities may explain why optimizing the inter-modal alignment loss can enhance intra-class discriminability to some extent—the learning of image embeddings is largely guided by the inherently discriminative text embeddings. Meanwhile, the gap between the two hyper-class still remains (See, e.g., Figure B.6a and Figure B.6b for comparison). In contrast, our method learns discriminative and well-balanced representations for both modalities.

#### B.6. Learning Curves

We plot the learning curves with respect to the clustering accuracy of our method on CIFAR-100, CIFAR-100, Stanford Cars and Flowers102 in Figure B.7. We can observe that our SSR<sup>2</sup>-GCD converges and achieves stable clustering results on “All” categories within 50 epochs.

#### B.7. Computation and Memory Costs

The Running time and memory costs on Flowers-102 in Table B.11. Note that  $\log \det(\cdot)$  is cheap to handle because its scale is kept to  $\min\{|B|, d\}$  due to  $\log \det(\mathbf{I} + \mathbf{Z}\mathbf{Z}^\top) =$

$\log \det(\mathbf{I} + \mathbf{Z}^\top\mathbf{Z})$ . Comparing to TextGCD, the increased costs of our SSR<sup>2</sup>-GCD is due to RTA in forward pass.